Nanostructures of Octadecyltrisiloxane Self-Assembled Monolayers Produced on Au(111) Using Particle Lithography

Jie-Ren Li and Jayne C. Garno*

Department of Chemistry and the Center for BioModular Multi-Scale Systems, Louisiana State University, Baton Rouge, Louisiana 70803

ABSTRACT Preparing high-quality self-assembled monolayers (SAMs) of organosilanes on conductive metal substrates such as gold is problematic because of the hydrophobic nature of the surface under ambient conditions. Trace amounts of water are required for a surface hydrolysis reaction to form siloxane bridges to the metal substrate. We describe an approach using sequential steps of ultraviolet (UV) irradiation, particle lithography, and chemical vapor deposition of octadecyltrichlorosilane (OTS) to successfully prepare silane nanostructures on Au(111) surfaces. Pretreatment of gold films with UV irradiation renders the surface to be sufficiently hydrophilic for particle lithography. Close-packed films of monodisperse latex mesospheres provide an evaporative mask to spatially direct the placement of nanoscopic amounts of water on surfaces. Vapor-phase organosilanes deposit selectively at areas of the surface containing water residues to produce millions of nanopatterns with regular thickness, geometry, and periodicity. Atomic force microscopy (AFM) images reveal that OTS binding is localized to areas defined by water residues. The spacing between adjacent nanopatterns is determined by the periodicity of the latex mask; however, the dimensions of the nanostructures are confined to a narrow contact area of the water meniscus, which surrounds the base of the latex spheres. The siloxane nanostructures on Au(111) furnish an excellent model surface for AFM characterizations, as demonstrated with current-sensing measurements.

KEYWORDS: organosilane • self-assembled monolayers • gold • particle lithography • vapor deposition • atomic force microscopy

INTRODUCTION

Self-assembled monolayers (SAMs) provide an ideal platform for engineering surfaces at the molecular level and provide a vehicle for investigating reactions on surfaces (1–3). Well-defined organosilane SAMs on oxide surfaces were first reported by Sagiv in 1980 (4). Since then, organosilane SAMs have become widely applied for surface passivation and photoresists (5–7). Organosilanes also provide a versatile molecular platform that can be applied for surface patterning and nanofabrication (8–12). The interfacial functionalities of organosilane SAMs are tailorable for the design of surface chemistries to attach various nanomaterials (13–16). The robust covalent nature of organosilanes offers extensive mechanisms for further steps of chemical modification for the design of surface chemistry at the nanoscale (17–21).

The precise mechanism for surface assembly of organosilanes is not fully understood and is complicated by parameters of sample preparation such as the nature of the immersion solvent and surface (22). Organosilane SAMs are formed through hydrolysis reactions to make bridging siloxane bonds that anchor to the surface and also cross-link to form interconnections with adjacent molecules. Water is known to have an essential role in the self-assembly of organosilanes on surfaces (23–28). Nanoscopic amounts of water are essential for initiating a surface hydrosilylation reaction; however, excess water can induce polymerization reactions to generate multilayers and branched structures. As silane SAMs are formed, there is a competition between the formation of Si–O bridges to adjacent molecules, connections to the substrate, or production of silanols, SiOH (4, 29, 30). Typical substrates used to prepare SAMs of organosilanes are silicon, quartz, glass, metal oxides, and mica (1, 3). For substrates that contain relatively few hydroxyl groups, such as mica(0001), prehydrolysis of organosilanes (31) or exposure of the surfaces to water vapor (32) has been used to effect the surface hydrosilylation.

There are sparse reports that evidence that organosilanes such as octadecyltrichlorosilane (OTS) can be prepared on gold substrates in ambient environments, and for these accounts, the surface coverage and quality of the organosilane films have not been documented with scanning probe characterizations. Previously, it was considered that surfaces with free hydroxyl groups were required to form SAMs of organosilanes. This view was adjusted when organized monolayers of OTS were shown to form on gold, which is a substrate devoid of hydroxyl groups (33–37). In these reports, it was demonstrated that OTS molecules assemble on a thin film of water adsorbed on the gold surface rather than on the gold substrate itself. Functionalized organosilanes such as (3-aminopropyl)triethoxysilane (APS) or trimethylsilylacetylene (TMSA) also have been reported to form SAMs on gold surfaces (38, 39). Reflection absorption infra-

red spectroscopy (RAIRS), ellipsometry, contact-angle, and quartz-crystal microbalance studies reveal that APS adsorbed on gold to yield multilayer films (38). For TMSA, scanning tunneling microscopy (STM) results indicate that SAMs of TMSA are generated with Si−Au chemical bonds (39). In the absence of water under ultrahigh-vacuum (UHV) conditions, it was demonstrated that alkylsilanes ($H_{2n+1}C_nSiH_3$) formed a monolayer on gold through Si−H bond activation when deposited at room temperature (40−42). Results with X-ray photoelectron spectroscopy reveal that the silicon head-groups attached to the gold surface to form a film. However, for samples prepared in UHV, characterizations with RAIRS and STM indicate that the alkyl chains form disordered monolayers as compared to alkanethiol SAMs.

The nature of gold surfaces limits applicability for surface reactions with organosilanes. Among the properties of gold surfaces, wettability has generated considerable controversy in literature reports (43−47). With different techniques applied to measure the wettability of gold under varied conditions, reports for the contact angle of gold surfaces range from 0 to 65° (43−45, 48−50). A hydrophilic gold surface can be obtained after tedious cleaning processes, such as exposure to oxygen plasma (34, 37, 51), piranha solution (52), or ultraviolet (UV) irradiation (53, 54). Gold surfaces were reported to have a contact angle of 0° immediately after removal from vacuum, which rapidly increased to 40° with exposure to the atmosphere (47). Under ambient conditions, complete wetting of gold is not achieved because of the adsorption of organic molecules from the environment (47). As a consequence, silanization of gold surfaces through hydrolysis to form dense, high-quality SAMs is problematic because of difficulties in achieving a consistent distribution of water throughout areas of the hydrophobic surface.

In this report, we present a facile high-throughput approach for preparing octadecyltrisiloxane nanostructures on surfaces of gold by combining particle lithography with vapor deposition of organosilanes (55). To improve the wettability of the Au(111) surface, the substrates were exposed to UV irradiation before depositing aqueous solutions of latex. Essentially, the evaporative masks of latex produced with particle lithography were used to define the surface sites of nanoscopic residues of water. Successful results for preparing OTS nanopatterns are demonstrated with contact-mode atomic force microscopy (AFM) characterizations. The conductive nature of the gold substrates further enabled protocols for current imaging and current-sensing AFM (CS-AFM) with the test platforms of OTS nanopatterns.

EXPERIMENTAL SECTION

Materials and Reagents. Octadecyltrichlorosilane (OTS) was purchased from Gelest (Morrisville, PA) and used without further purification. Certified particle size standards of polystyrene latex (300 nm) were obtained from Duke Scientific (Palo Alto, CA). The latex particles were washed twice by centrifugation with deionized water (Milli-Q; Millipore, Bedford, MA) to remove possible contaminants such as charge stabilizers or surfactants. Gold thin films evaporated on mica substrates with a thickness

of 150 nm were obtained from Agilent Technologies Inc. (Chandler, AZ). Ethanol (ACS grade; Pharmco, Aaper, TX) and toluene (reagent grade; EMD Chemical Inc., Gibbstown, NJ) were used to rinse samples.

AFM. Topography, friction, and CS-AFM images were acquired using an Agilent 5500 scanning probe microscope equipped with *PicoScan* v5.3.3 software (Agilent Technologies Inc., Chandler, AZ). Silicon nitride tips with an average force constant of 0.5 N m^{-1} were used for contact-mode AFM imaging in air (MSCT-AUHW; Veeco Instruments, Inc., Camarillo, CA). The silicon nitride probes used for contact-mode AFM were coated with OTS to minimize tip−surface adhesion, and the total forces applied for imaging were <1 nN. CS-AFM was used to map the sample conductance while operating in contact mode. Different bias voltages (+6, 0, and −6 V) were applied to the samples for acquiring CS-AFM data. The tips used for CS-AFM were highly doped silicon probes with a Ti/Pt coating with an average force constant of 0.2 N m^{-1} (ANSCMPC; Nanoscience Instruments, Inc., Phoenix, AZ). Images were processed using *Gwyddion* (version 2.10) open-source software supported by the Czech Metrology Institute, which is freely available on the internet (56).

Particle Lithography. Particle lithography combined with vapor deposition was used to generate octadecyltrisiloxane nanostructures on gold substrates. Particle lithography, also known as nanosphere lithography, uses the natural arrangement of spherical particles to produce arrays of nanostructures on surfaces (57−59). Monodisperse particles self-assemble into periodic structures on flat surfaces to guide the deposition of various materials, such as SAMs (55, 60−62), proteins (63−65), inorganic materials (66, 67), and polymers (68, 69). An overview of the steps for particle lithography with vapor deposition is shown in Figure 1. To prepare nanostructures, the gold surfaces were exposed to UV light (254 nm) for 4 h. Next, a 20 μL volume of an aqueous solution containing (2 % w/v) polystyrene latex particles (300 nm) was immediately deposited on clean gold substrates with a micropipet (Figure 1 A). A view of a 300 nm latex mask is shown within the area of the circle (topograph). The sample was then dried in ambient conditions (25 °C, relative humidity ∼60 %) for 2 h. As water evaporates during drying, capillary forces draw the latex spheres together to form organized crystalline layers (Figure 1A). Trace residues of water persist at the base of the latex spheres to form a circular meniscus. The dried film of latex was then used as an evaporative mask for vapor deposition of organosilanes (Figure 1B). To accomplish the vapor deposition, the colloidal masks were placed into a glass vessel containing 300 μL of neat OTS. The reaction vessel (a glass jar) was sealed and placed in an oven at 70 °C for 8 h to generate a vapor. During heating, the OTS vapors attach to the exposed areas not masked by latex spheres and bind covalently at sites containing water residues (Figure 1B). The mask of latex particles was removed by sonication in ethanol for 2 min followed by further rinsing with deionized water, ethanol, and toluene (Figure 1C). Nanopatterns of OTS were not removed from the surface by the rinsing procedure.

A control sample of an OTS film on Au(111) was prepared to match the conditions of the samples prepared by particle lithography, omitting the particle lithography step. To prepare control samples, the gold substrates were exposed to UV light of (254 nm) for 4 h. A volume of 20 μL of deionized water was then placed on the UV-treated gold substrates using a micropipet. The sample was dried in ambient conditions (25 °C, relative humidity ∼60 %) until the water evaporated (∼35 min). The gold substrate was then placed inside a glass vessel containing 300 μL of OTS. The vessel was sealed and placed in an oven and heated at 70 °C for 8 h. After vapor deposition was completed, the samples were rinsed with deionized water, ethanol, and toluene.
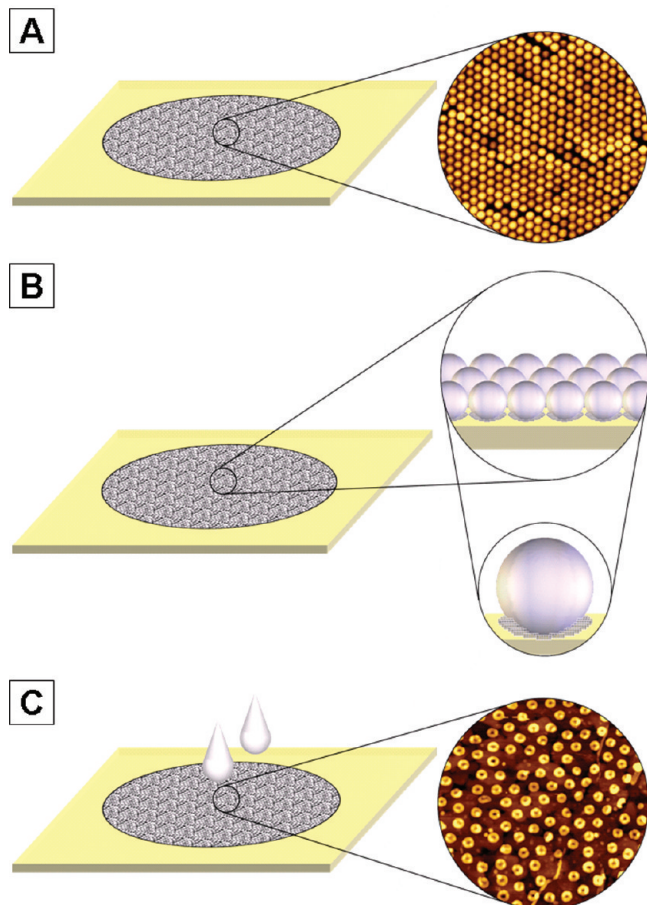
FIGURE 1. Steps of particle lithography for fabricating organosilane nanostructures on Au(111). (A) A mask of latex spheres was prepared on a UV-treated gold substrate. (B) A mask of latex spheres appeared after organosilane vapor deposition. (C) After rinsing, latex masks were selectively removed to reveal organosilane nanopatterns.

RESULTS AND DISCUSSION

Successful examples of ring-shaped nanostructures of OTS produced on Au(111) using particle lithography combined with chemical vapor deposition (300 nm latex masks) are demonstrated in Figure 2. Arrays of octadecyltrisiloxane nanostructures with ring-shaped morphologies are observed on the gold surfaces with irregularly shaped terraces. An AFM topograph of 893 rings produced within a $10 \times 10 \, \mu m^2$ area is shown in Figure 2A, which would scale to approximately 10^8 rings per cm^2. The arrangement of the organosilane rings conforms to the periodicity of the latex mask. The pores of the rings pinpoint the locations where the individual latex particles were rinsed away. The long-range order and organization of octadecyltrisiloxane rings are apparent, evidencing a few defects produced by missing particles. The hydrophobic nature as well as local defects of the gold substrate influences the long-range periodicity and packing density of latex mesospheres. A few faint line patterns of OTS formed at the edges of gold terraces, defining the areas of the substrate that contained water residues.

The changes in surface chemistry between the organosilane rings and the gold substrate are viewed in the frictional force image of Figure 2B. Friction images result from differences in adhesion between the tip and sample, providing a
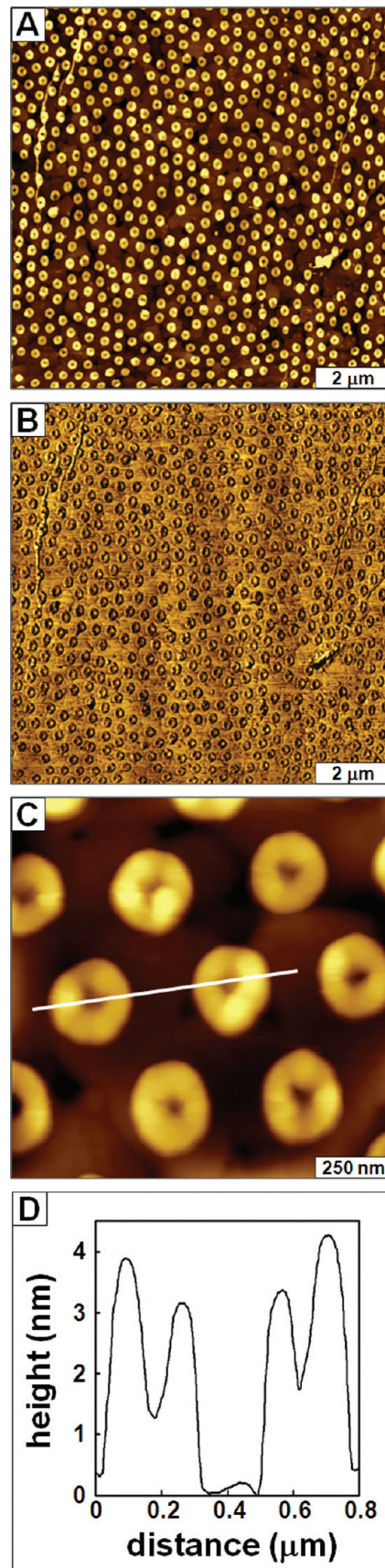

FIGURE 2. Ring-shaped nanostructures of OTS prepared on gold using particle lithography combined with vapor deposition: (A) wide-area topograph; (B) corresponding frictional force image; (C) zoom-in view; (D) cursor profile for the line in panel C.
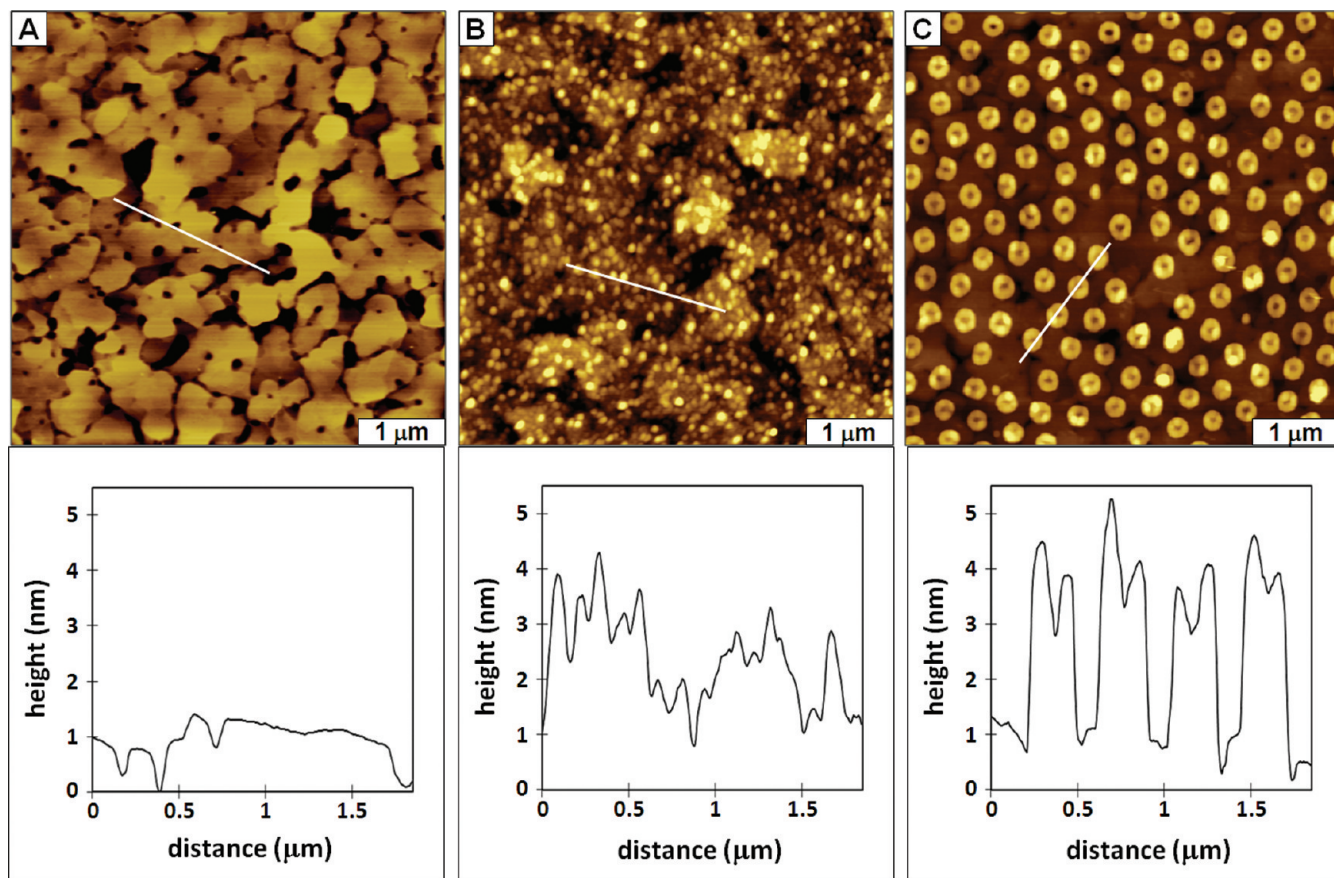
FIGURE 3. Water-directed assembly of OTS on oxidized surfaces of Au(111) viewed for 5×5 μm^2 AFM topographs: (A) untreated Au(111) substrate; (B) OTS film produced using vapor deposition without steps of particle lithography; (C) ring-shaped nanostructures of OTS produced by vapor deposition through latex masks.

sensitive map of the changes in surface chemistry. Friction images also can reflect changes resulting from surface topography such as edge effects. The outlines of the nano-patterns predominate for the ring patterns, with bright or dark contrast at the pattern edges, as the tip travels up or down across the patterns. The edge effects are produced for the frictional force image because of changes in tip−surface interactions as the probe is scanned over the nanostructures, providing a precise outline of the ring geometries. A hex-agonal arrangement of rings is visible in the zoom-in topog-raphy image (Figure 2C) and corresponding cursor profile (Figure 2D). The shapes and dimensions of the nanopatterns are exquisitely reproducible at the nanoscale, with regular diameters of 246 ± 6 nm and pore areas inside the rings of 48 ± 4 nm. The lateral periodicity measures 321 ± 13 nm between neighboring nanostructures, which matches closely with the 300 nm diameter of the latex masks. The average height of the rings is 3.7 ± 0.6 nm, which is slightly higher than the theoretical height of OTS (2.8 nm). In the zoom-in AFM image and cursor profile, it is apparent that at the nanoscale the rings vary by as much as 1.2 nm in height. The height variability indicates branching within the siloxane network.

A control experiment was conducted without using a latex mask to further elucidate the role of water and surface wettability for the self-assembly of OTS on Au(111). The

Au(111) substrates were similarly exposed to UV light, as in Figure 3; however, the surface was moistened by applying a drop of water (20 μL) and allowing it to dry. The water droplet was dried in ambient conditions for 45 min and then placed into a sealed vessel containing 300 μL of OTS for heated vapor deposition. Representative images of similar size areas of a bare gold substrate, control sample, and OTS nanopatterns are compared side-by-side with contact-mode AFM topographs in Figure 3. The morphology typical of a vacuum-deposited gold/mica is revealed in Figure 3A for the untreated Au(111) surface, exhibiting irregularly shaped terrace domains. The root-mean-square roughness mea-sured 2.9 nm for the area shown. After vapor deposition, a clustered, irregular morphology was revealed, with incom-plete surface coverage of random island protrusions through-out terrace and step edge areas (Figure 3B). Protrusion islands of OTS are evident throughout areas of the surface, measuring 2.2 ± 0.4 nm in height, referencing shallower areas of the surface as a baseline. The baseline areas are not bare gold; the sample contains near-complete surface cover-age of an octadecyltrisiloxane film. The thickness of the OTS film is variable, which is likely caused by nanoscale varia-tions in the distribution of water present on the surface. A comparable size area with octadecyltrisiloxane nanostruc-tures is presented in Figure 3C, showing 132 rings of OTS. The nanostructures cover $\sim$33 % of the surface and exhibit
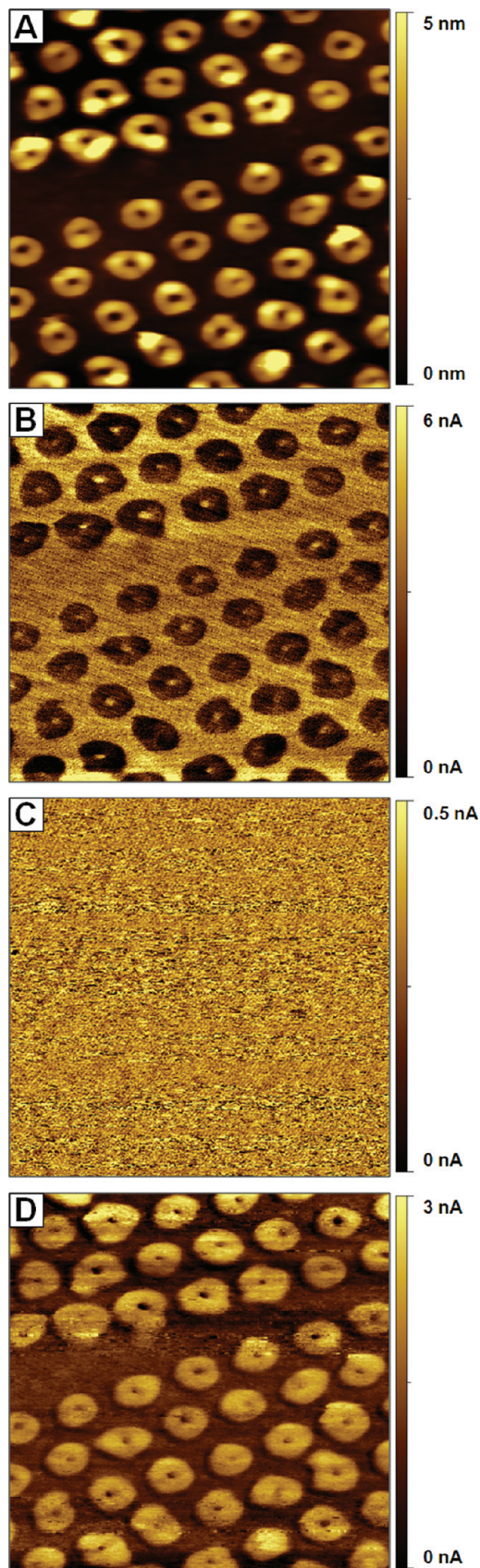
FIGURE 4. Evolution of changes in CS-AFM images acquired with various sample bias voltages. (A) Topography image of OTS nanopatterns produced with 300 nm latex masks. CS-AFM images of octadecyltrisiloxane rings acquired with (B) −6 V, (C) 0 V, and (D) +6 V for the same scan area.

remarkably uniform thickness and geometries. Long-range order and regular spacing between the ring patterns of OTS are apparent throughout areas of the 1×1 cm^2 sample, with few defects.

Characterizations with CS-AFM were used to evaluate the conductivity of the OTS ring patterns (Figure 4). For CS-AFM, a bias voltage is applied to the substrate, and the current through the molecular film is measured when the AFM tip is placed in direct contact with the surface. For comparative reference, a topography image (2.5×2.5 μm^2) acquired using the same metal-coated probe is presented in Figure 4A, which displays 51 rings of OTS arranged in diagonal rows and columns. The third horizontal row is shifted slightly downward in alignment, providing a convenient in situ landmark for comparing the different data channels. The same scan area was imaged successively for the current frames. Current images display highly conductive regions as bright or dark features, depending on the bias polarity. As the polarity of the sample bias was switched from −6 to +6 V, the contrast correspondingly changed. For measurements with CS-AFM, the metal-coated tip remains at virtual ground as a bias is applied to the sample. The current signal is positive when the sample surface is biased negatively, and reversed contrast is shown for the opposite bias polarity. The bright areas of Figure 3B indicate that uncovered regions of the gold surface are highly conductive. When a positive voltage is applied to the surface, the current likewise becomes negative. When the bias is zero, no contrast is visible for the current image (Figure 4C). With a positive bias, the bright contrast is attributable to less conductive areas, as in Figure 4D. The current image in Figure 4D was acquired at +6 V and displays reverse contrast compared to Figure 4B.

The regions of the nanopatterns exhibit relatively homogeneous contrast in current images, in correspondence with observations of the regular surface topography and highly uniform thickness of the rings. The robust ring structures of OTS appear to be densely packed and were not observed to degrade despite repetitive AFM imaging in contact mode or at elevated bias. The current contrast of the small pore areas within the rings matches the substrate, which is evidence that the mesosphere masks were cleanly removed to expose bare areas of the gold substrate. Nanopatterns of OTS prepared on Au(111) are suitable for investigations of charge transport and the development of molecular-scale measurements. Gold surfaces also furnish advantages as electrodes or for etching processes.

The AFM probe can be placed directly on the surface of individual nanostructures to acquire local I−V spectra (Figure 5). Three rings were selected to evaluate the conductivity. The nanostructures selected for acquiring I−V spectra are identified in the topography image of Figure 5A. As the sample bias was scanned from −10 to +10 V, slightly asymmetric, nonlinear I−V profiles were observed when the forward and reverse bias sweeps were compared (Figure 5B). The measurements match well with previously reported I−V spectra (70−72). A sharp peak was observed between −4 and −5 V, which indicates the oxidation of OTS SAMs
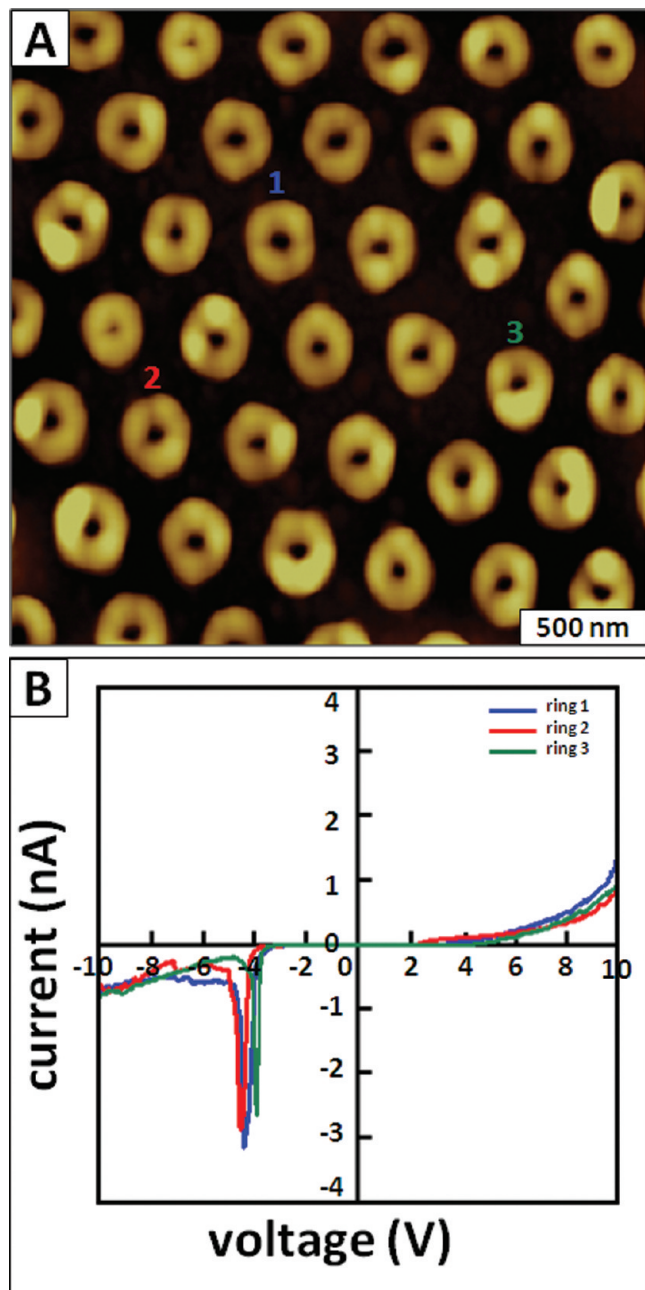
FIGURE 5. CS-AFM measurements of octadecyltrisiloxane rings: (A) Topograph of the area selected for measurements; (B) *I*−*V* profiles acquired for three octadecyltrisiloxane nanostructures.

(72). The maximum current measured 1 ± 0.4 nA in both negative and positive bias regions, which displays the expected insulating nature of the alkyl chains of OTS (73, 74). The bias values at the onset of current conduction from the *I*−*V* profiles were used to establish the conditions for acquiring current images for parts B and D of Figure 3.

Approaches based on scanning probe lithography (SPL) have also been applied to produce organosilane nanopatterns (20, 75−77). Methods of SPL provide exquisite nanoscale resolution and enable us to subsequently visualize the surface morphology with great detail. However, with SPL the patterns are fabricated one at a time by slow serial writing processes, which are not easily scalable for

the high throughput and reproducibility needed for device manufacture. Approaches with particle lithography provide advantages of high throughput and reproducibility for generating millions of organosilane nanostructures, based on simple bench chemistry procedures. The size, shape, and spacing of features can be precisely controlled with mesoparticle masks. Once the experimental conditions are optimized, dozens of samples prepared with the selected conditions exhibit identical nanoscale morphologies. Multiple samples were prepared, and images of Figures 2A and 4A are taken from samples prepared separately on different days. The AFM views shown are representative of multiple areas throughout the surface.

The poor wettability of gold substrates in ambient conditions was addressed by UV light exposure, which is known to improve surface hydrophilicity and remove organic contaminants. During UV irradiation, gold surfaces are oxidized but recover hydrophilicity (33, 54, 78, 79). In the presence of trace residues of water on oxidized gold surfaces, OTS molecules are hydrolyzed and reduce gold oxide with $SiCl_3$ moieties (33, 34). Typically, trace amounts of water are required to form densely packed organosilane monolayers. The quality of organosilane SAMs depends on the degree of hydration on surfaces. For a substrate devoid of hydroxyl groups such as Au(111), UV surface treatment was used to improve the adhesion of water. With particle lithography, nanoscopic residues of water could be uniformly arranged and distributed throughout areas of the surface by latex mesoparticles to direct the binding of organosilanes.

With latex masks, nanoscopic amounts of water are spatially confined and retained underneath the spheres localized to a meniscus area at the base where the mesoparticles meet the surface. The masks were prepared by drying an aqueous solution of latex particles on the UV-treated gold substrate under ambient conditions. During the drying step, most of the water evaporates from the surface and only tiny residues of water persist to form a uniform, circular meniscus near the base of the latex mesospheres. The outer surfaces of latex spheres have spongelike properties to absorb water and retain small amounts of moisture when dried (80−83). When OTS vapor is introduced to the latex masks, hydrolysis takes place selectively where water is present within the circular areas of the liquid meniscus. The shapes of the nanostructures correspond to the areas with a water meniscus near the base of the latex mesoparticles.

Surfaces with well-defined nanopatterns provide a platform for further chemical steps to adsorb proteins, nanoparticles, or other nanomaterials. By the selection of organosilanes with designed functionalities, nanoscale control of surface chemistry can be achieved. After organosilane nanopatterns are fabricated using particle lithography, uncovered areas of the Au(111) substrate are available for further steps of chemical patterning or etching. Circular organosilane nanostructures can be used as boundaries to isolate and direct adsorption of new

materials in well-defined arrangements. Alkanethiol SAMs also can be deposited to backfill uncovered areas of the Au(111) substrate for defining surface selectivity at the nanoscale.

CONCLUSION

A robust, high-throughput nanofabrication approach was accomplished using steps of particle lithography combined with chemical vapor deposition to reproducibly generate periodic nanostructures of OTS on surfaces of Au(111). Pretreatment of the gold substrates with UV irradiation was used to improve surface wettability. Millions of OTS nanopatterns are produced with exquisitely regular and uniform geometries and arrangement. CS-AFM measurements of nanostructures reveal the insulating nature of octadecylsiloxane on conductive gold surfaces.

REFERENCES AND NOTES

(1) Ulman, A. *Chem. Rev.* **1996**, *96*, 1533–1554.
(2) Love, J. C.; Estroff, L. A.; Kriebel, J. K.; Nuzzo, R. G.; Whitesides, G. M. *Chem. Rev.* **2005**, *105*, 1103–1169.
(3) Onclin, S.; Ravoo, B. J.; Reinhoudt, D. N. *Angew. Chem., Int. Ed.* **2005**, *44*, 6282–6304.
(4) Sagiv, J. *J. Am. Chem. Soc.* **1980**, *102*, 92–98.
(5) Thames, S. F.; Panjnani, K. G. *J. Inorg. Organomet. Polym. Mater.* **1996**, *6*, 59–94.
(6) Hozumi, A.; Ushiyama, K.; Sugimura, H.; Takai, O. *Langmuir* **1999**, *15*, 7600–7604.
(7) Brzoska, J. B.; Benazouz, I.; Rondelez, F. *Langmuir* **1994**, *10*, 4367–4373.
(8) Dulcey, C. S.; Georger, J. H.; Krauthamer, V.; Stenger, D. A.; Fare, T. L.; Calvert, J. M. *Science* **1991**, *252*, 551–554.
(9) Xia, Y. N.; Mrksich, M.; Kim, E.; Whitesides, G. M. *J. Am. Chem. Soc.* **1995**, *117*, 9576–9577.
(10) Lercel, M. J.; Craighead, H. G.; Parikh, A. N.; Seshadri, K.; Allara, D. L. *Appl. Phys. Lett.* **1996**, *68*, 1504–1506.
(11) Ivanisevic, A.; Mirkin, C. A. *J. Am. Chem. Soc.* **2001**, *123*, 7887–7889.
(12) Hoeppener, S.; Maoz, R.; Sagiv, J. *Nano Lett.* **2003**, *3*, 761–767.
(13) Grabar, K. C.; Allison, K. J.; Baker, B. E.; Bright, R. M.; Brown, K. R.; Freeman, R. G.; Fox, A. P.; Keating, C. D.; Musick, M. D.; Natan, M. J. *Langmuir* **1996**, *12*, 2353–2361.
(14) Chrisey, L. A.; Lee, G. U.; Oferrall, C. E. *Nucleic Acid Res.* **1996**, *24*, 3031–3039.
(15) Mooney, J. F.; Hunt, A. J.; McIntosh, J. R.; Liberko, C. A.; Walba, D. M.; Rogers, C. T. *Proc. Natl. Acad. Sci. U.S.A.* **1996**, *93*, 12287–12291.
(16) Gao, Y. F.; Koumoto, K. *Cryst. Growth Des.* **2005**, *5*, 1983–2017.
(17) Wasserman, S. R.; Tao, Y. T.; Whitesides, G. M. *Langmuir* **1989**, *5*, 1074–1087.
(18) Balachander, N.; Sukenik, C. N. *Langmuir* **1990**, *6*, 1621–1627.
(19) Maoz, R.; Cohen, S. R.; Sagiv, J. *Adv. Mater.* **1999**, *11*, 55–61.
(20) Maoz, R.; Frydman, E.; Cohen, S. R.; Sagiv, J. *Adv. Mater.* **2000**, *12*, 725–731.
(21) Killampalli, A. S.; Ma, P. F.; Engstrom, J. R. *J. Am. Chem. Soc.* **2005**, *127*, 6300–6310.
(22) Wen, K.; Maoz, R.; Cohen, H.; Sagiv, J.; Gibaud, A.; Desert, A.; Ocko, B. M. *ACS Nano* **2008**, *2*, 579–599.
(23) Angst, D. L.; Simmons, G. W. *Langmuir* **1991**, *7*, 2236–2242.
(24) Le Grange, J. D.; Markham, J. L.; Kurkjian, C. R. *Langmuir* **1993**, *9*, 1749–1753.
(25) Britt, D. W.; Hlady, V. *J. Colloid Interface Sci.* **1996**, *178*, 775–784.
(26) Vallant, T.; Brunner, H.; Mayer, U.; Hoffmann, H.; Leitner, T.; Resch, R.; Friedbacher, G. *J. Phys. Chem. B* **1998**, *102*, 7190–7197.
(27) Krasnoslobodtsev, A. V.; Smirnov, S. N. *Langmuir* **2002**, *18*, 3181–3184.
(28) Wu, K.; Bailey, T. C.; Willson, C. G.; Ekerdt, J. G. *Langmuir* **2005**, *21*, 11795–11801.
(29) Carson, G. A.; Granick, S. *J. Mater. Res.* **1990**, *5*, 1745–1751.
(30) Tripp, C. P.; Hair, M. L. *Langmuir* **1992**, *8*, 1120–1126.
(31) Kessel, C. R.; Granick, S. *Langmuir* **1991**, *7*, 532–538.
(32) Schwartz, D. K.; Steinberg, S.; Israelachvili, J.; Zasadzinski, J. A. N. *Phys Rev. Lett.* **1992**, *69*, 3354–3357.
(33) Finklea, H. O.; Robinson, L. R.; Blackburn, A.; Richter, B.; Allara, D.; Bright, T. *Langmuir* **1986**, *2*, 239–244.
(34) Sabatani, E.; Rubinstein, I.; Maoz, R.; Sagiv, J. *J. Electroanal. Chem.* **1987**, *219*, 365–371.
(35) Allara, D. L.; Parikh, A. N.; Rondelez, F. *Langmuir* **1995**, *11*, 2357–2360.
(36) Vallant, T.; Brunner, H.; Kattner, J.; Mayer, U.; Hoffmann, H.; Leitner, T.; Friedbacher, G.; Schugerl, G.; Svagera, R.; Ebel, M. *J. Phys. Chem. B* **2000**, *104*, 5309–5317.
(37) Sabatani, E.; Rubinstein, I. *J. Phys. Chem.* **1987**, *91*, 6663–6669.
(38) Kurth, D. G.; Bein, T. *Langmuir* **1995**, *11*, 3061–3067.
(39) Katsonis, N.; Marchenko, A.; Taillemite, S.; Fichou, D.; Chouraqui, G.; Aubert, C.; Malacria, M. *Chem.—Eur. J.* **2003**, *9*, 2574–2581.
(40) Owens, T. M.; Nicholson, K. T.; Holl, M. M. B.; Suzer, S. *J. Am. Chem. Soc.* **2002**, *124*, 6800–6801.
(41) Owens, T. M.; Suzer, S.; Holl, M. M. B. *J. Phys. Chem. B* **2003**, *107*, 3177–3182.
(42) Owens, T. M.; Ludwig, B. J.; Schneider, K. S.; Fosnacht, D. R.; Orr, B. G.; Holl, M. M. B. *Langmuir* **2004**, *20*, 9636–9645.
(43) White, M. L. *J. Phys. Chem.* **1964**, *68*, 3083–3085.
(44) Bewig, K. W.; Zisman, W. A. *J. Phys. Chem.* **1965**, *69*, 4238–4242.
(45) Erb, R. A. *J. Phys. Chem.* **1968**, *72*, 2412–2417.
(46) Gardner, J. R.; Woods, R. *J. Electroanal. Chem.* **1977**, *81*, 285–290.
(47) Smith, T. *J. Colloid Interface Sci.* **1980**, *75*, 51–55.
(48) Zettlemoyer, A. C. *J. Colloid Interface Sci.* **1968**, *28*, 343–369.
(49) White, M. L.; Drobek, J. *J. Phys. Chem.* **1966**, *70*, 3432–3436.
(50) Erb, R. A. *J. Phys. Chem.* **1965**, *69*, 1306–1309.
(51) Rubinstein, I.; Steinberg, S.; Tor, Y.; Shanzer, A.; Sagiv, J. *Nature* **1988**, *332*, 426–429.
(52) Evans, S. D.; Sharma, R.; Ulman, A. *Langmuir* **1991**, *7*, 156–161.
(53) Sondag-Huethorst, J. A. M.; Fokkink, L. G. J. *Langmuir* **1992**, *8*, 2560–2566.
(54) King, D. E. *J. Vac. Sci. Technol., A* **1995**, *13*, 1247–1253.
(55) Li, J. R.; Garno, J. C. *Nano Lett.* **2008**, *8*, 1916–1922.
(56) Klapetek, P. N. D. Czech Metrology Institute, Brno, Czech Republic, 2007, http://gwyddion.net/.
(57) Xia, Y. N.; Gates, B.; Yin, Y. D.; Lu, Y. *Adv. Mater.* **2000**, *12*, 693–713.
(58) Haynes, C. L.; Van Duyne, R. P. *J. Phys. Chem. B* **2001**, *105*, 5599–5611.
(59) Yang, S. M.; Jang, S. G.; Choi, D. G.; Kim, S.; Yu, H. K. *Small* **2006**, *2*, 458–475.
(60) McLellan, J. M.; Geissler, M.; Xia, Y. N. *J. Am. Chem. Soc.* **2004**, *126*, 10830–10831.
(61) Geissler, M.; McLellan, J. M.; Chen, J. Y.; Xia, Y. N. *Angew. Chem., Int. Ed.* **2005**, *44*, 3596–3600.
(62) Bae, C.; Shin, H. J.; Moon, J.; Sung, M. M. *Chem. Mater.* **2006**, *18*, 1085–1088.
(63) Garno, J. C.; Amro, N. A.; Wadu-Mesthrige, K.; Liu, G. Y. *Langmuir* **2002**, *18*, 8186–8192.
(64) Li, J. R.; Henry, G. C.; Garno, J. C. *Analyst* **2006**, *131*, 244–250.
(65) Ngunjiri, J. N.; Daniels, S. L.; Li, J. R.; Serem, W. K.; Garno, J. C. *Nanomedicine* **2008**, *3*, 529–541.
(66) Jiang, P.; Bertone, J. F.; Colvin, V. L. *Science* **2001**, *291*, 453–457.
(67) Tessier, P.; Velev, O. D.; Kalambur, A. T.; Lenhoff, A. M.; Rabolt, J. F.; Kaler, E. W. *Adv. Mater.* **2001**, *13*, 396–400.
(68) Jiang, P.; Hwang, K. S.; Mittleman, D. M.; Bertone, J. F.; Colvin, V. L. *J. Am. Chem. Soc.* **1999**, *121*, 11630–11637.
(69) Jiang, P.; McFarland, M. J. *J. Am. Chem. Soc.* **2004**, *126*, 13778–13786.
(70) Aswal, D. K.; Lenfant, S.; Guerin, D.; Yakhmi, J. V.; Vuillaume, D. *Small* **2005**, *1*, 725–729.

(71) Aswal, D. K.; Lenfant, S.; Guerin, D.; Yakhmi, J. V.; Vuillaume, D. *Anal. Chim. Acta* **2006**, *568*, 84–108.

(72) Chauhan, A. K.; Aswal, D. K.; Koiry, S. P.; Gupta, S. K.; Yakhmi, J. V.; Surgers, C.; Guerin, D.; Lenfant, S.; Vuillaume, D. *Appl. Phys. A* **2008**, *90*, 581–589.

(73) Fontaine, P.; Goguenheim, D.; Deresmes, D.; Vuillaume, D.; Garet, M.; Rondelez, F. *Appl. Phys. Lett*. **1993**, *62*, 2256–2258.

(74) Vuillaume, D.; Boulas, C.; Collet, J.; Davidovits, J. V.; Rondelez, F. *Appl. Phys. Lett*. **1996**, *69*, 1646–1648.

(75) Choi, I.; Kang, S. K.; Lee, J.; Kim, Y.; Yi, J. *Biomaterials* **2006**, *27*, 4655–4660.

(76) Headrick, J. E.; Armstrong, M.; Cratty, J.; Hammond, S.; Sheriff, B. A.; Berrie, C. L. *Langmuir* **2006**, *21*, 4117–4122.

(77) Gu, J. H.; Yam, C. M.; Li, S.; Cai, C. Z. *J. Am. Chem. Soc*. **2004**, *126*, 8098–8099.

(78) Pireaux, J. J.; Liehr, M.; Thiry, P. A.; Delrue, J. P.; Caudano, R. *Surf. Sci*. **1984**, *141*, 221–232.

(79) Ron, H.; Rubinstein, I. *Langmuir* **1994**, *10*, 4566–4573.

(80) Neto, J. M. M.; Cardoso, A. L. H.; Testa, A. P.; Galembeck, F. *Langmuir* **1994**, *10*, 2095–2099.

(81) Chen, Y. Y.; Ford, W. T.; Materer, N. F.; Teeters, D. *Chem. Mater*. **2001**, *13*, 2697–2704.

(82) Tan, S. S.; Sherman, R. L.; Qin, D. Q.; Ford, W. T. *Langmuir* **2005**, *21*, 43–49.

(83) Kim, A. J.; Manoharan, V. N.; Crocker, J. C. *J. Am. Chem. Soc*. **2005**, *127*, 1592–1593.